Targeting the Conformational Transitions of MDM2 and MDMX: Insights into Dissimilarities and Similarities of p53 Recognition

Antonio Macchiarulo,[†] Nicola Giacchè,[†] Andrea Carotti,[†] Massimo Baroni,[‡] Gabriele Cruciani,[‡,§] and Roberto Pellicciari*,[†]

Dipartimento di Chimica e Tecnologia del Farmaco, Università di Perugia, via del Liceo 1, 06123 Perugia, Italy, Molecular Discovery Ltd., 215 Marsh Road, Pinner, Middlesex HA55NE, England, and Laboratory for Chemometrics and Cheminformatics, Department of Chemistry, Università di Perugia, via Elce di Sotto 10, 06123 Perugia, Italy

Received April 28, 2008

MDM2 and MDMX are oncogenic homologue proteins that regulate the activity and stability of p53, a tumor suppressor protein involved in more than 50% of human cancers. While the large body of experiments so far accumulated has validated MDM2 as a therapeutically important target for the development of anticancer drugs, it is only recently that MDMX has also become an attractive target for the treatment of tumor cells expressing wild type p53. The availability of structural information of the N-terminal domain of MDM2 in complex with p53-derived peptides and inhibitors, and the very recent disclosure of the crystal structure of the N-terminal domain of MDMX bound to a p53 peptide, offer an unprecedented opportunity to provide insight into the molecular basis of p53 recognition and the identification of discriminating features affecting the binding of the tumor suppressor protein at MDM2 and MDMX. By using coarse graining simulations, in this study we report the exploration of the conformational transitions featured in the pathway leading from the apo-MDM2 and apo-MDMX states to the p53-bound MDM2 and p53-bound MDMX states, respectively. The results have enabled us to identify a pool of diverse conformational states of the oncogenic proteins that affect the binding of p53 and the presence of conserved and *non*-conserved interactions along the conformational transition pathway that may be exploited in the design of selective and dual modulators of MDM2 and MDMX activity.

INTRODUCTION

The interaction between the tumor suppressor protein p53 and negative or positive regulators is critical to maintain in check the pro-apoptotic activity of p53 and thus cell cycle arrest.[1] More than 50% of human cancers have been associated with mutations of p53 and impairments of its regulatory pathway.[2−5] The core module of the p53 regulatory pathway has long been considered the interaction between the oncogenic protein MDM2 and the transactivation function of the tumor suppressor protein. MDM2 is an E3 ubiquitin ligase enzyme that, upon binding to p53, leads the tumor suppressor protein to the proteasomal degradation. Since MDM2 is also a target gene of the transcriptional activity of p53, this protein−protein interaction constitutes an example of a negative feedback loop where the induced expression of MDM2 gene by p53, in turn, downregulates the activity of p53. On this basis, the physical interaction between MDM2 and p53 has been largely studied and validated as a key target for the development of new cancer therapeutic strategies. In particular, the structural information accumulated so far on the N-terminal domain of MDM2, in complex with p53-derived peptides, with small druglike inhibitors, and in its unbound form, has constituted the starting point for the development of structure-based inhibitor design and successful virtual screening strategies.[6−8]

Table 1. Composition of the Systems Used for Simulating the Conformational Transitions from the apo-State to the p53-Bound State of MDM2 and MDMX

system	models	no. of residues	no. of atoms
A	**A1**: apo-form of MDM2 + p53	101	1548
	A2: p53-bound form of MDM2	101	1548
B	**B1**: apo-form of MDMX + p53	101	1548
	B2: p53-bound form of MDMX	101	1548

Not withstanding the fact that the discovery of MDMX (also known as MDM4) occurred in 1996 by Shvarts et al.,[9] only recently has scientific interest in this oncogenic protein emerged for its independent regulatory role in controlling p53 activity. The interaction of MDMX with p53 does not target the tumor suppressor protein for degradation but rather inactivates its transcriptional activity. Conversely to MDM2, MDMX is constitutively expressed in cells, and its expression is not regulated by p53.[9,10] It should also be noted that MDMX is also able to interact with MDM2 through the RING domain.[11] The consequence of this interaction is that MDMX is targeted for proteasomal degradation by MDM2.[12−14]

A number of studies have demonstrated that the oncogenic proteins MDM2 and MDMX are unable to compensate the

* Corresponding author phone: +39 075 585 5120; fax: +39 075 585 5114; e-mail: rp@unipg.it.
[†] Dipartimento di Chimica e Tecnologia del Farmaco, Università di Perugia.
[‡] Molecular Discovery Ltd.
[§] Laboratory for Chemometrics and Cheminformatics, Department of Chemistry, Università di Perugia.

10.1021/ci800146m CCC: $40.75
Published on Web 10/01/2008

cell for the loss of the other and that they synergistically regulate nonoverlapping functions of p53.[15−22]

In the light of these observations, a dynamic model of regulation of p53 activity where MDMX acts as a major inhibitor of p53 transcriptional activity and MDM2 regulates p53 and MDMX stabilities has been proposed.[3,23,24] This model relies on a preferential affinity of MDM2/MDMX interaction during stress condition of the cell which, upon stress relief, shifts to MDM2/p53 and MDMX/p53 interactions.

Overexpression of the MDMX gene has been observed in 40% of tumor cell lines.[25] Furthermore, there is also a specificity of MDMX or MDM2 overexpression within different types of tumor cells.[3] For instance, increased expression of the MDMX protein has been recently associated with human retinoblastomas.[26] The therapeutical potential of targeting both MDM2 and MDMX in cancer has been very recently demonstrated through the use of a nonselective peptide inhibitor. Intratumoral injection of such a peptide in mouse tumor xenografts was able to simultaneously disrupt the interactions of MDM2 and MDMX with p53 and efficiently suppress cancer cell proliferation.[27]

While the above evidence fosters the notion that development of dual-inhibitors of MDM2 and MDMX interaction may be crucial to the achievement of a full activation of p53, the availability of selective MDM2 and MDMX chemical tools may prove instrumental in fulfilling the pharmacological characterization and target validation of these oncogenic proteins in different cancer cell lines that specifically overexpress MDMX or MDM2.

To date, few studies of inhibitors of the MDM2/p53 interaction showing MDMX inhibition have been reported. Recent studies indicate that despite the sequence homology shared by MDM2 and MDMX, the MDM2 inhibitor nutlin-3 (**1**) is not able to fully rescue p53 from MDMX binding.[28−30] In addition, the recent disclosure of the crystal structure of MDMX in complex with p53 demonstrated that the binding site in MDMX is narrower then MDM2 albeit presenting the same minimal motif in the interaction with p53.[31]

With the aim of investigating the structural and conformational elements controlling the specificity of p53 recognition by MDM2 and MDMX, we report herein the characterization of the conformational transitions leading from the apo-MDM2 and apo-MDMX states to the p53-bound MDM2 and p53-bound MDMX states.

METHODS

Preparation of the apo- and p53-Bound Models. In order to study the conformational transitions leading to p53 recognition, models of the apo-states of MDM2 (model A1) and MDMX (model B1) and the structures of the p53-bound of these proteins (models A2 and B2) were prepared using the Schrödinger Suite 2007.[32]

In particular, conformational model 12 of the apo-MDM2 NMR structure (pdb code: 1Z1M)[33] was used to arrange the apo-state of the protein (model A1) since it has a packed fold where the N-terminal portion of the MDM2 protein adopts a "closed lid" position over the p53 binding site, whereas the p53-bound complex (pdb code: 1T4F)[34] was used to prepare model A2 being the p53-bound complex of MDM2 with the best resolution (1.90 Å). In order to have the same sequence length (residues 18−109) in both the apo- and p53-bound models (A1, A2), the conformation 12 of the apo-MDM2 NMR structure (pdb code: 1Z1M) was modified by deleting the first 17 residues at the N-terminal (residues 1−17) and the last 10 residues at the C-terminal (residues 110−119) tails. Similarly, the crystal structure 1T4F was modified by adding 5 residues at the N-terminal tail (residues 18−22) and deleting the last residue (residue 110) at the C-terminal tail. The main-chain and side-chain conformations of the added residues were assigned on the basis of the experimental conformations adopted by the same residues in the crystal structure 1T4E where they are solved. In order to finalize the apo-state of MDM2 in model A1, the p53 peptide of the crystal structure 1T4F was merged at approximately 30 Å from the p53 binding cleft of the apoprotein. Since the apo- state of the MDMX protein is experimentally not available, a homology model was built using a sequence alignment between the human MDM2 and MDMX (see the Supporting Information, Figure s1). The modified conformational model 12 of the apo-MDM2 (model A1) was used as a template for the assignment of the atomic coordinates. The program SCAP was employed for the homology modeling study.[35]

In line with model A1, the apo-state of MDMX in model B1 was finalized by adding the p53 peptide from the crystal structure 1T4F at approximately 30 Å from the binding cleft of the apoprotein. The p53-bound state of MDMX (model B2) was arranged using the recently available crystal structure of MDMX in complex with p53 (pdb code: 2Z5T).[31] This structure was totally humanized using the human sequence of MDMX and the program SCAP. The original p53 peptide was also replaced by fitting the p53 peptide of the MDM2 crystal structure 1T4F into the experimental pose. The resulting p53-bound state of MDMX was defined as model B2. Again, to ensure the same length of sequences (residues 18−108) in the apo- and p53-bound models of MDMX (B1, B2), the crystal structure 2Z5T was modified deleting the first residue at the N-terminal tail (residue 17 of the human MDMX sequence) and the last residue at the C-terminal tail (residue 109 of the human MDMX sequence).

All the obtained models (A1, A2, B1, and B2) were energetically refined using the Protein Preparation Wizard workflow of *Maestro*.[32] The hydrogen bonding network of each model was optimized using the server Molprobity[36] without the flipping option. The models were also geometrically checked by the Molprobity, Anolea, and Verify3D servers (see the Supporting Information, Figure s2).[37,38]

As a general comment, it should be mentioned that the above procedure of model preparation allowed us to consider a portion of the N-terminal lid of MDM2 and MDMX in our simulations.

It has been demonstrated, indeed, that such a region (residues 17−24) is important in controlling the access of p53 to the relative binding site and that its sequence differs notably between the two oncogenic proteins.[39,40] Unfortunately, we were not able to consider the entire N-terminal region (residues 1−24) as far as the largest part of its sequence that has been solved in the p53-bound state of MDM2 contains only seven residues (residues 18−24) as observed in the crystal structure 1T4E.

Spatial Coarse Graining Simulations. Spatial coarse graining (SCG) simulations were performed using the

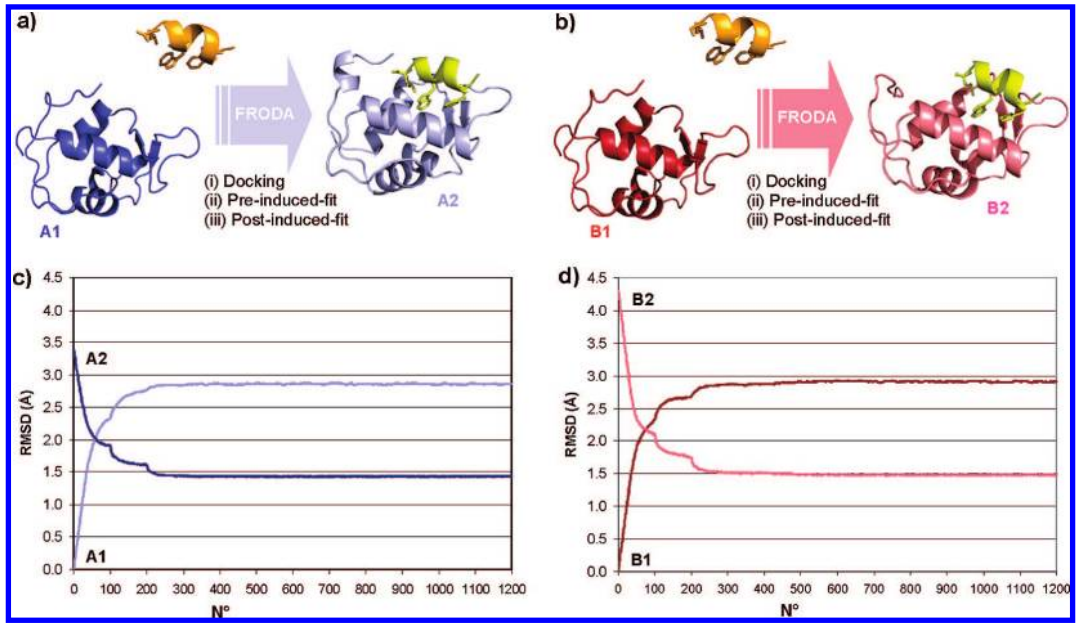

Figure 1. (a, b) The general scheme adopted for the targeted simulation to sample the conformational transitions from the apo form to the p53-bound of MDM2 (blue) and MDMX (red). (c, d) The rmsd deviations from the starting model (A1, B1) and the arrival model (A2, B2) are calculated during the targeted simulations of MDM2 (blue and light-blue) lines and MDMX (red and light-red lines).

command-line version of FIRST 6.0 and the Framework Rigidity Optimized Dynamic Algorithm (FRODA).[41]

This approach, developed by Thorpe and co-workers, consists of using a graph-theoretical algorithm to construct a graph network on the basis of the protein structure. Residue atoms represent the nodes of the network, while the edges between the nodes are the covalent and noncovalent bonds observed in the protein structure. Noncovalent bonds consist of the hydrogen bonds and hydrophobic interactions of the protein. Once these interactions are identified and described by the algorithm in terms of constrains, a network is constructed and analyzed in order to identify rigid regions. These latter are identified through the application of the program FIRST (Floppy Inclusions and Rigid Substructure Topography). No relative motion is allowed within these rigid regions, but they can only move as rigid bodies with six degrees of freedom. The list of atoms belonging to the rigid regions during the simulations are provided in the Supporting Information (file Rigid_Regions.xls).

Subsequently, the program FRODA generates several conformations of the protein using random Monte Carlo dynamics. In a targeted simulation, FRODA is instructed to sample the entire conformational space available to the flexible regions of the protein that lie between a starting conformational model (A1, B1) and a final conformational model (A2, B2). Since the FRODA approach does not use any force field, it is not able to give information on the energy associated with the different conformational states of the protein. With respect to molecular dynamic simulations, however, it has as main advantages the low computational cost and the increased speed required to have a qualitative view of the conformational space of the protein and to identify the molecular events leading the transitions between different conformational states.

In the two SCG simulations, the default basic options of FRODA were used with the activation of specific flags that are reported in the Supporting Information (flags.doc). The construction of the noncovalent bond network was carried out setting an energy H-bond cutoff of −1.0 kcal/mol. Each SCG simulation consisted of a targeted simulation followed by a free simulation. In the targeted simulation, the conformational transitions leading from the apo-states (models A1, B1) to the p53-bound states (models A2, B2) of MDM2 and MDMX are explored using three consecutive runs of FRODA, namely docking (i), pre-induced-fit (ii), and post-induced-fit (iii).

In the second run of FRODA, namely the pre-induced-fit, all the hydrophobic interactions tethering the side chains of Tyr100 in MDM2 and Tyr99 in MDMX were removed by editing the relative "phobes.out" files into "phobes.in" files. These latter were used by FIRST to identify the resulting rigid regions of the proteins and construct new graph networks for the second run of FRODA. The third run of FRODA, namely the post-induced-fit, was arranged starting from the last conformation obtained in the pre-induced-fit and using FIRST to construct a new graph network for each of the two targeted simulations. It should be mentioned that both the pre- and post-induced-fit runs were necessary to more closely reproduce the experimental p53-bound MDM2 and MDMX conformations. This is because the presence of hydrophobic interactions tethering Tyr100 in MDM2 and Tyr99 in MDMX wrongly assigned these residues to the rigid regions of the proteins, thus hampering a correct reproduction of their relative conformational movements.

The final conformational states of p53-bound MDM2 and MDMX obtained from the targeted simulations were used as input structures to perform the free simulations with an additional run of FRODA. During this run, rigid regions and flexible regions of the proteins moved without any target constraint in compliance with their rules of motion.

A total of 2200 protein conformations were saved along each of the SCG simulations of MDM2 and MDMX for further analysis.

Statistical Analysis. The root-mean-square deviations (rmsd) of the atomic coordinates of the 2.2×10^3 MDM2

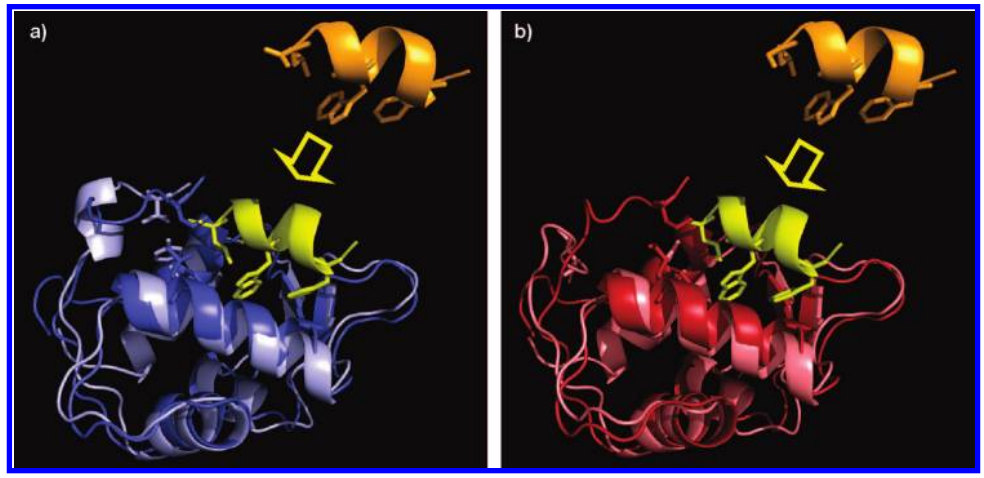

Figure 2. Docking run of FRODA: p53 (orange and yellow) is progressively docked into the binding site of MDM2 and MDMX. (a) Superposition of the apo model (blue) and the p53-docked model (light-blue) of MDM2. (b) Superposition of the apo model (red) and the p53-docked model (light-red) of MDMX.

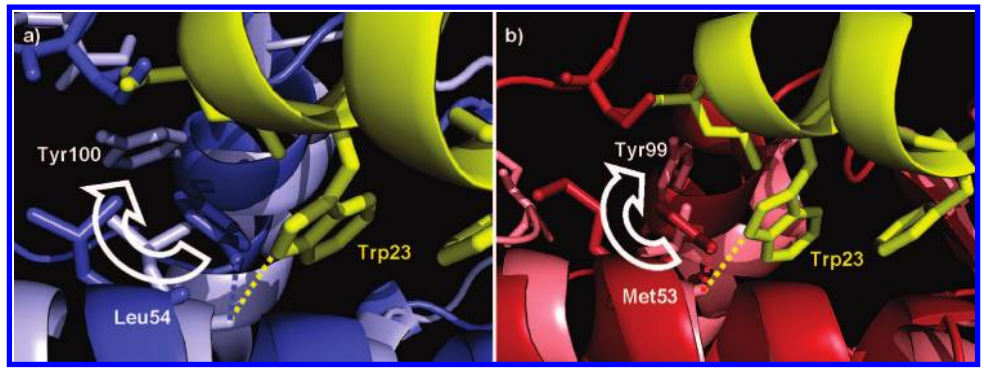

Figure 3. Pre- and postinduced-fit runs of FRODA. The intramolecular interactions between Tyr100 and Leu54 in MDM2 (a, dotted blue line) and Tyr99 and Met53 in MDMX (b, dotted red line) are broken to be replaced by intermolecular interactions with Trp23 of p53 (yellow). The large movement featuring the side chain of Tyr100 and Tyr99 upon p53 recognition is highlighted with an arrow.

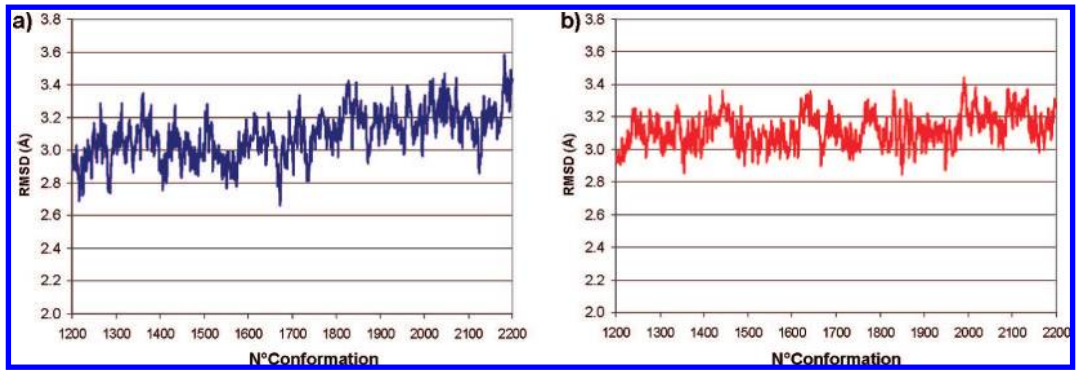

Figure 4. The rmsd deviations from the starting models (A1, B1) calculated during the free simulations of MDM2 (a) and MDMX (b).

and MDMX conformations were calculated using the GROMACS tools.[42]

The clustering analysis was performed using the g-cluster (ver. 3.3.99) tool as implemented in GROMACS with rmsd values calculated on all atoms in the range of residues 25−109 and 25−108 for MDM2 and MDMX, respectively. An optimal rmsd cutoff of 1.03 Å was calculated and used in order to have roughly the same number of clusters in MDM2 and MDMX. The conformation lying in the center of each cluster was selected as representative of the group (see the Supporting Information, Tables s1 and s2).

These rmsd values were also used to construct the distance matrix necessary to perform a Multidimensional Scaling (MDS) analysis.[43] The aim of this method is to build a mapping of a series of individual conformations from the distance matrix between these individuals. To build an optimal representation, the MDS algorithm minimizes a criterion called "Stress". The closer the stress to zero, the better the representation. The combined MDS maps (Figure 4) of MDM2 and MDMX conformations were built using an rmsd matrix calculated over the backbone atoms of the proteins.

The fluctuation of residues was calculated using g-RMSF as implemented in GROMACS using the following templates: 1Z1M (model 12 and model 24); 1T4F; conf-02111 of the free simulation. These template models were selected being the vertexes of a square drawn to cover the four

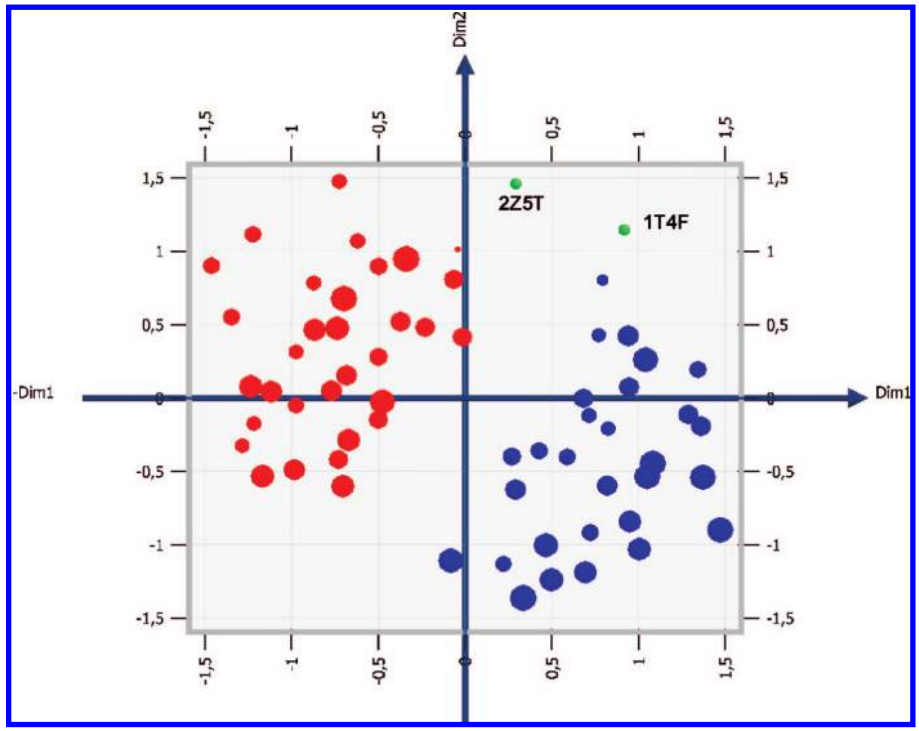

Figure 5. MDS map (Kruskal Stress = 0.352) combining the representative clusters of MDM2 (blue spheres) and MDMX (red spheres) conformations as resulting from the targeted and free simulations. The size of the sphere is proportional to the Monte Carlo step of the simulation. The positions occupied by the crystal structures of p53-bound MDM2 (pdb code: 1T4F) and MDMX (pdb code: 2Z5T) are marked with green spheres.

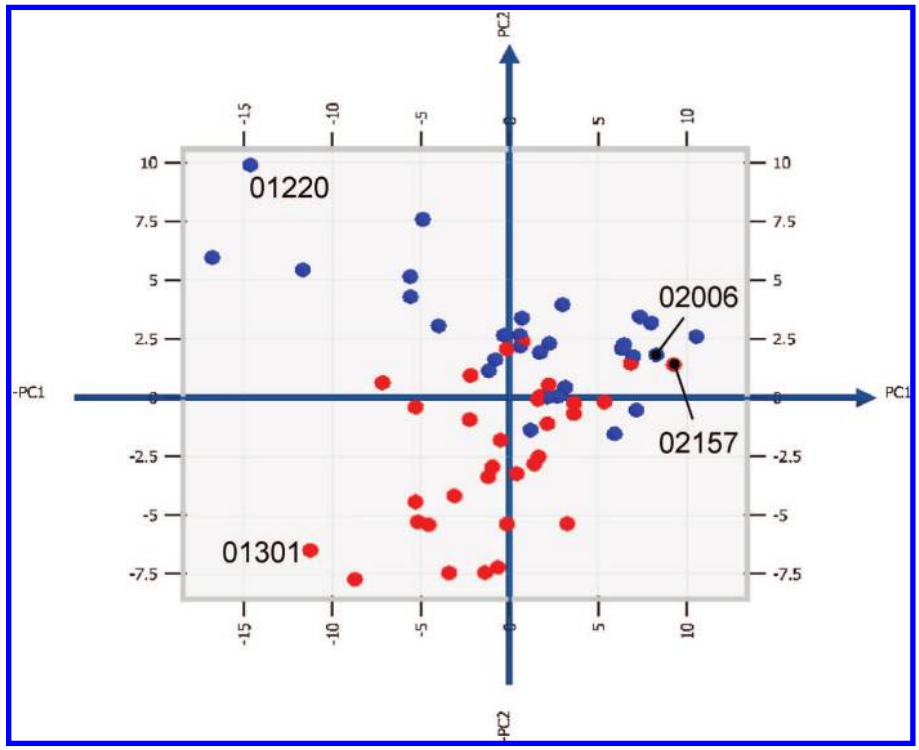

Figure 6. Plot of the scores of MDM2 (blue) and MDMX (red) conformations along the first and second components of the PCA study. The conformations selected for the visualization of the molecular interaction fields are labeled.

quadrants of the MDS map and whose lines were parallel respectively to the abscissa and ordinate axes. The differences between the mutual fluctuations of residues in the four templates were used to identify the amino acids that sustained large conformational movements with increasing values of the first and second dimensions of the MDS map (see the Supporting Information, Figure s3). The analysis of the interactions between MDM2, MDMX, and p53 during the SCG simulations was carried out using the program LigPlot.[44]

Molecular Interaction Field Analysis. A number of computational techniques have been developed to exploit the relevant information from the X-ray crystallographic structures. One of the pioneering approaches in this field was the

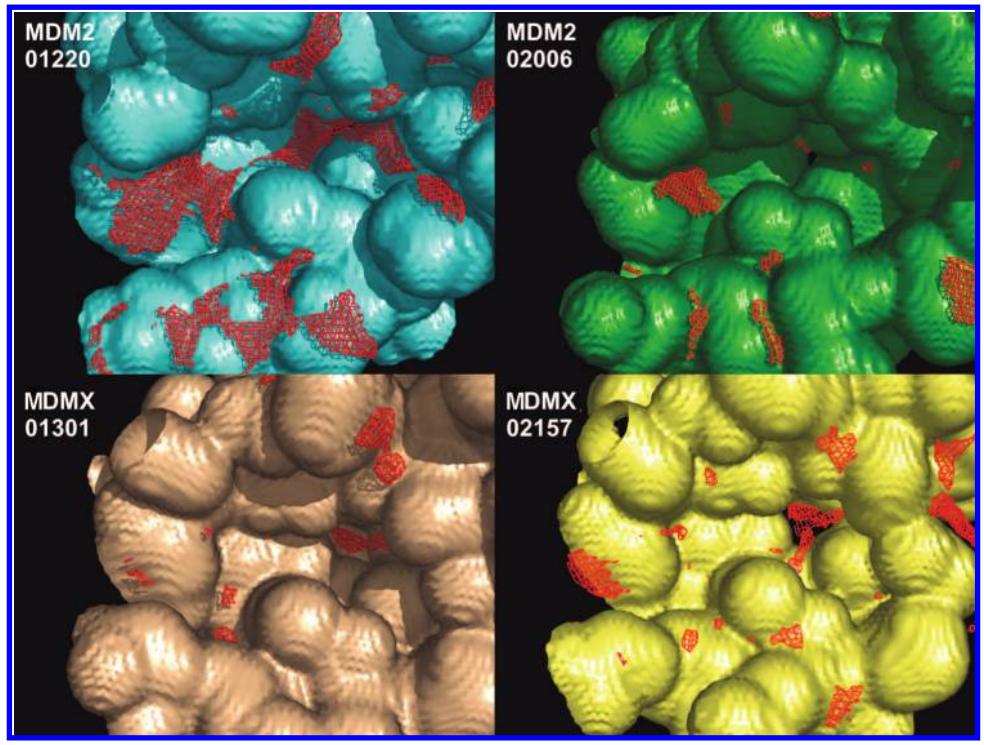

Figure 7. Molecular interaction fields produced by the hydrophobic probe into the binding site of different MDM2 and MDMX conformations (see Figure 6 for the localization of the four conformations in the score plot).

GRID program. GRID molecular probes are carefully parametrized using X-ray experimental data. By computing the energetic interaction of the probes with the protein structure and different positions of a chemical probe on a 3D grid, molecular interaction fields (MIFs) are generated. The target may be a molecule or a macromolecule or even a molecular complex.

Originally, GRID-derived MIFs were developed to determine energetically favorable binding sites on macromolecules in order to predict where ligands bind to biological macromolecules. Thereby, MIFs can guide structure-based ligand design whenever the target is a protein, a therapeutic agent, or other biologically important macromolecule, gaining a better insight to the factors affecting the binding helps in the design of improved ligands.

However, GRID MIFs are also frequently applied to docking procedures or molecular dynamics studies, specially when combined with a new computational approach called FLAP (Fingerprint for Ligand And Protein)[45] able to compare and cluster protein families into target classes, without any bias from previous knowledge. Thus MIFs can not only be explored using molecular graphics but also collected and studied to obtain more and more relevant information (see Figure 7 for a MIFs view of MDM2 and MDMX pockets).

It is worth mentioning that FLAP utilizes only Molecular Interaction Fields (MIFs) and not the protein 3D structure, atom distances, or other structural information and does not require protein superposition, alignment, or knowledge-based comparison. Differently from previously reported works for protein similarity and clustering, FLAP allows protein−protein comparison based on the psychochemical description of the complementary part of protein binding sites, the so-called "ligand space". Therefore the psychochemical description of the "ligand space" gives a common frame of reference for comparing different proteins or, such as in this paper, different snapshots of the same proteins.

RESULTS

In the targeted simulation, FRODA was instructed to sample the conformational space lying between the apo-conformational models (starting models A1 and B1, Figure 1a-b) and the p53-bound conformational model of the proteins (arrival models A2 and B2, Figure 1a,b).

During the three runs of the targeted simulation (docking and pre- and postinduced fit), the root-mean-square deviation (rmsd) calculated from the starting models increased, whereas it decreased from the arrival models until reaching a plateau value of 1.43 Å and 1.48 Å, respectively, for MDM2 and MDMX (Figure 1c,d).

While in the docking run of FRODA, p53 was brought progressively closer to the binding site of MDM2 and MDMX (Figure 2), in the pre- and post-induced-fit runs of FRODA the intramolecular interactions of the proteins were broken to be replaced by the intermolecular interactions with p53 (Figure 3a,b). The pre-induced-fit run was particularly important as far as it instructed FRODA about the route to follow in order to move the proteins from models A1, B1 to models A2, B2 (see the Method and Discussion sections for more details).

The final conformational states achieved by the targeted simulations of p53-bound MDM2 and MDMX were instrumental in performing a free simulation using an additional run of FRODA without employing the targeting models of the proteins (models A2, B2). The aim of this task was to sample the conformational space of the final resulting p53 complexes of MDM2 and MDMX (Figure 4).

While a number of 1.2×10^3 conformational states out of 1.2×10^4 calculated conformations were saved during

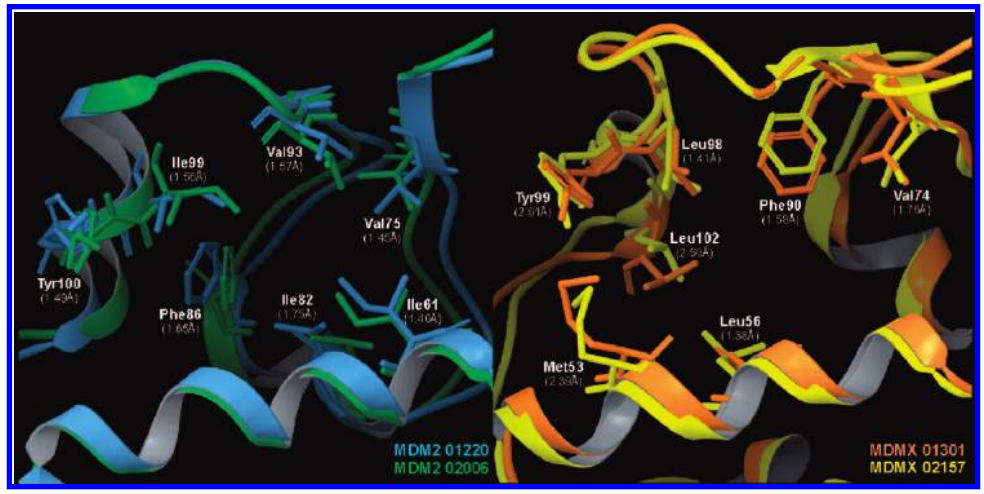

Figure 8. Most interesting conformational differences (rmsd > 1.38 Å) of residues that contribute to the diverse hydrophobic interactions produced into the p53 binding site of two MDM2 (confs. 01220, 02006) and MDMX (confs. 01301, 02157) conformations (see Figure 6 for the localization of the four conformations in the score plot).

the targeted simulations for each system, a number of 1.0×10^3 conformational states out of 1.0×10^6 produced conformations were stored during the free simulation (see the Method section for details). These conformations were clustered on the basis of their rmsd values calculated over all the atomic coordinates of MDM2 (residues 25−109) and MDMX (residues 25−108) without considering the p53 peptide. The clustering analysis of MDM2 simulations yielded 29 groups of diverse conformations, with one group being from the targeted simulations and the remaining 28 groups being from the free simulation. The clustering analysis of MDMX simulations produced 32 groups of conformations, with one group being from the targeted simulation and 31 groups being from the free simulation. Interestingly, each group contained a number of conformations contiguous in the conformational transition from apo- MDM2 and MDMX to p53-bound MDM2 and MDMX (see the Supporting Information, Table s1) and could be traced back to specific Monte Carlo steps of the SCG simulations.

A distance matrix was built using the rmsd values between the backbone of the conformations at the center of the clusters, and a Multidimensional Scaling (MDS) was instrumental in providing a combined map of the MDM2 and MDMX conformational states (Figure 5). In the MDS map, the size of the sphere is proportional to the Monte Carlo steps required to find the representing conformation in the simulation.

The analysis of the interactions between MDM2, MDMX, and p53 showed that the number of hydrophobic contacts is significantly higher than the number of polar interactions, with MDM2 being on average favored over MDMX ($MDM2_{nonpolar} = 33.03 \pm 5.94$; $MDMX_{nonpolar} = 25.16 \pm 6.64$; $MDM2_{polar} = 1.41 \pm 0.68$; $MDMX_{polar} = 1.13 \pm 0.34$) in the recognition of p53.

A principal component analysis carried out on FLAP molecular interaction field descriptors calculated into the p53 binding cleft of MDM2 and MDMX conformations supported this notion (Figure 6). The first principal component was unable to distinguish MDM2 from MDMX conformers, but the second component successfully divided the data set into three main clusters containing MDM2 conformations (high PC scores), MDMX conformation (low PC scores), and mixed conformations (medium PC scores). The analysis of the FLAP fingerprint showed that the second component was mainly related to hydrophobic interactions, therefore confirming that it is mainly the hydrophobic interaction pattern which distinguishes between MDM2 and MDMX conformations (Figure 7). Figure 8 shows the most interesting conformational differences of residues that contribute to the diverse hydrophobic interactions produced into the p53 binding site of some selected MDM2 and MDMX conformations.

DISCUSSION

The process of protein−protein recognition is believed to be divided into two major molecular mechanisms, responsible respectively for complex formation and stabilization.[46] The molecular mechanism underlining protein complex formation is ascribed to the direct docking of the protein monomers, while the mechanism of complex stabilization is mediated by random collisions of the monomers that overcome the high thermodynamic barriers followed by fixation of the formed complex. Several data indicate that the first of these mechanisms requires directional forces such as hydrogen bonds and electrostatic forces, whereas the mechanism of stabilization is additionally determined by hydrophobic forces (see ref 17 and references therein).

The aim of this work was to investigate the structural and conformational elements controlling the specificity of p53 recognition by MDM2 and MDMX, using SCG simulations. Thus, according to the proposed double mechanism of protein−protein interaction, we used a targeted simulation moving from the apo- MDM2 and MDMX states to the p53-bound MDM2 and MDMX states followed by a free simulation of the resulting complexes, with the former describing the protein complex formation and the latter depicting the stabilization of the complexes.

Inspection of the experimental apo- (pdb code: 1Z1M) and p53-bound structures (pdb code: 1T4F) of MDM2, together with consideration of literature data,[33,39,47] revealed that three conserved residues, namely Ile19, Leu54, and Tyr100 (MDM2 numbering), play a pivotal role in the conformational rearrangements of the p53 binding site of MDM2. In all the NMR models of apo-MDM2, the conformation of Ile19 remains stable through the formation of hydrophobic

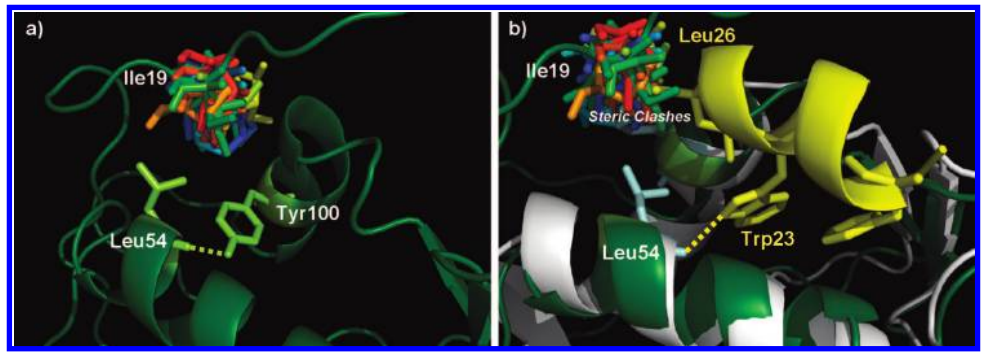

Figure 9. The adopted p53 recognition route. (a) Superposition of all conformations of Ile19 as observed in the NMR structure of the apo MDM2 (pdb code: 1Z1M). The hydrogen bond between the side chain of Tyr100 and the carbonyl group of Leu54 is marked. (b) Superposition of the p53-bound crystal structure (pdb code: 1T4F, white) and the apo-form of MDM2 (pdb code: 1Z1M, green). Steric clashes between Ile19 and Leu26 of p53 indicate a possible displacement from the binding cleft of the former residue upon p53 recognition. The hydrogen bond between Tyr100 and Leu54 is no longer present in the p53-bound crystal structure where it is replaced by the intermolecular hydrogen bond between the carbonyl group of Leu54 and the indolic ring of Trp23 (yellow sticks).

interactions, whereas the conformation of Tyr100 is stabilized through hydrogen bonding interactions with the carbonyl group of the backbone of Leu54 (Figure 9a). Conversely, in the crystal structure of p53-bound MDM2, while Ile19 is displaced away from the p53 binding cleft by the presence of Leu26 from p53, the intramolecular interaction between Tyr100 and Leu54 is broken and replaced by the intermolecular hydrogen bond that involves the carbonyl group of Leu54 and the indolic ring of Trp23 from p53 (Figure 9b). These conformational movements suggest an experimental route that is exploited by MDM2 to move from the apo-state to the p53-bound state. Thus, according to this route, steric clashes between Leu26 of p53 and Ile19 of MDM2 force the latter residue to move away from the binding cleft in order to make room to host p53. Simultaneously, in approaching the binding cleft of MDM2, p53 induces the displacement of Tyr100 of MDM2 from the intramolecular hydrogen bond with Leu54 and promotes the formation of a intermolecular hydrogen bond between the indolic ring of Trp23 and the carbonyl group of Leu54.

In order to adopt this route in our simulations, we have removed all the hydrophobic interactions tethering the side chains of Tyr100 in MDM2 and Tyr99 in MDMX during the pre-induced-fit run of the targeted simulation (see Method and Result sections for details). This procedure has been used to allow maximum conformational freedom for residue Tyr100 (and Tyr99 in MDMX) and, in turn, to trigger the breaking of the intramolecular interactions of the p53 binding site for the correct formation of the intermolecular interactions with p53.

At the end of the targeted and free simulations of MDM2 and MDMX, more than 1.0×10^6 conformations had been explored and 2.2×10^3 conformational states saved. These conformations were further reduced using a clustering analysis, and only the conformations at the center of the resulting clusters were stored, yielding respectively 29 unique conformations of MDM2 and 32 conformations of MDMX.

It should be mentioned that the majority of the representative clustered conformations arise from the free simulation, since the conformations of the targeted runs have been generated with the use of restraints and sampled to a less extend.

The inspection of Figure 5 reveals that MDM2 and MDMX adopt different conformations to bind p53. This may be in agreement with the observation that the p53 binding cleft of MDMX is narrower than the one of MDM2.[31] Thus, diverse conformational rearrangements take place in the two oncogenic proteins allowing the p53 peptide to be accommodated in two binding clefts endowed with different size. This result has been further confirmed by running two additional simulations, using the approaches applied in this study, on two known MDMX mutants with modified p53 recognition: $MDMX^{Met53Val}$ and $MDMX^{Tyr99Thr}$.[31] The results indicate that also these mutants adopt different conformational profiles to bind p53 (see the Supporting Information, Figure s4), supporting the hypothesis that the recognition of p53 is influenced by the conformational plasticity of the protein.

In order to gain further insights into the conformational elements that regulate the interaction with p53, the representative conformations obtained from the MDM2 simulations have been combined in a MDS map with the experimental conformations of the apo-, inhibitor-bound, and p53-bound states of the protein (Figure 10). The inspection of this map indicates the presence of two conformational aspects of MDM2 that are involved in p53 recognition. These are described by the two dimensions of the map with the first dimension (x axis) being ascribed to the movement of residues 31, 33, 71, 72, 78, 105−109 (fluctuation ± 0.5 Å) and the second dimension (y axis) being ascribed to a larger region of residues comprising positions 25, 26, 35, 36, 38, 43, 46, 64, 66, 70−72, 86, 87, 93, 94−97, 101, 102, 104−106, 108 (fluctuation ± 0.5 Å).

From a careful inspection of the map, we may speculate that the two dimensions reflect the double mechanism of protein−protein interaction, with the second dimension (y axis) depicting the conformational aspect of complex formation and the first dimension (x axis) describing the conformational aspect of complex stabilization. Indeed, all the experimental apo-state of MDM2 have low values of the y axis. Raising the value of the ordinate, the conformation of the MDM2 monomer gets closer to the ligand-bound conformations and the complex with p53 can be formed. Conversely, raising the value of the abscissa, several p53-bound conformations of MDM2 may be generated by random collisions that are instrumental to the stabilization of the complex. It is worth noting that the cluster of the conformations produced during the targeting simulation of MDM2

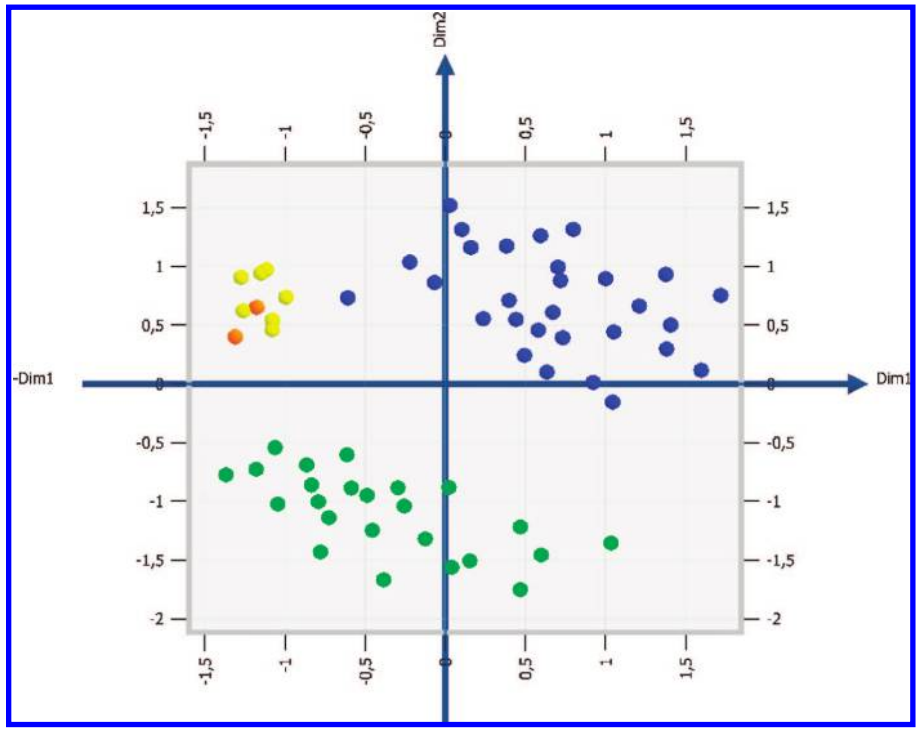

Figure 10. MDS map (Kruskal Stress = 0.226) combining the representative clusters of MDM2 conformations (blue spheres) and the experimental apo (green spheres), p53-bound (orange spheres), and ligand-bound (yellow spheres) structures of MDM2.

lies close to the experimental static conformation of the ligand-bound MDM2 complexes, whereas the conformations of p53-bound MDM2 resulting from the free simulation have higher values of the *x* axis (Figure 10). This observation may reflect the use of restraints during the targeting runs.

The analysis of the intermolecular interactions carried out using LigPlot indicates that the recognition of p53 is favored in MDM2 with respect to MDMX, with the first protein counting more hydrophobic contacts than the second. This is in agreement with the experimental data reporting that the p53 peptide used for our simulations is 2-fold more active at MDM2 ($K_D = 0.45\ \mu M$) than MDMX ($K_D = 35\ \mu M$).[31] The nature of the molecular recognition of p53 is mainly hydrophobic as resulting from the large number of hydrophobic contacts compared to polar interactions.

In line with this observation, a principal component analysis of the molecular interaction fields produced by the p53 binding cleft of MDM2 and MDMX conformations clearly indicates that the scores of the second component, encoding the hydrophobic interaction, differentiate MDM2 from MDMX, with the former assuming higher positive values than the latter (Figures 6 and 7). These differences are associated with unique conformational arrangements of residues into the p53 binding cleft of MDM2 and MDMX (Figure 8).

This result supports the idea that MDM2 and MDMX adopt different hydrophobic interactions for the recognition of p53. However, as far as polar interactions contribute to the complex formation, we have also analyzed which residues are mainly involved in hydrogen bonding with p53 in MDM2 and MDMX conformations. This analysis reveals that one residue of each oncogenic protein is involved in the hydrogen bonding with p53 in all conformations (Figure 11): Leu54 in MDM2 and Met53 in MDMX which make a hydrogen bond with Trp23 of p53. While the key role of Leu54 in

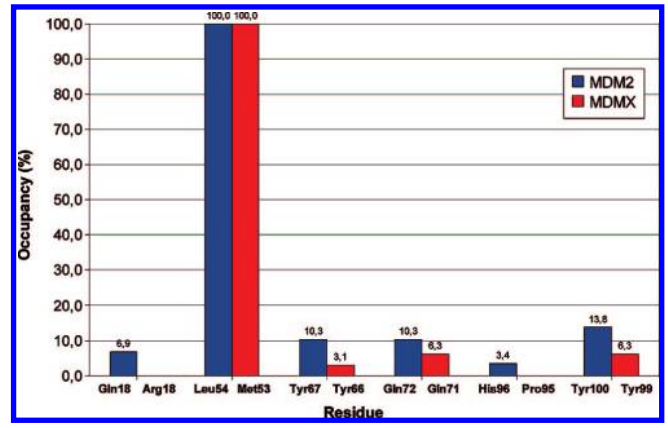

Figure 11. Analysis of the occupancy (expressed as percentage) of the hydrogen bond interactions anchoring p53 during the targeted and free simulations of MDM2 and MDMX.

MDM2 has been discussed in a number of reports,[33,39,47] it has been recently demonstrated that the MDMX mutant Met53Val reduces the affinity of the wild type protein to p53. Thus, it is conceivable that the branched side chain of valine hampers the hydrogen bond formation involving its carbonyl group of the main chain with p53. The occupancy in the conformations of the hydrogen bonds mediated by other residues, comprising Tyr100 of MDM2 and Tyr99 of MDMX, is below the 15%, hence they have only a marginal role in the stabilization of the complex. These data are in agreement with the reported observation that the mutation of Tyr99 into threonine in MDMX, shortening the polar side chain, does not significantly affect the recognition of p53.[31]

Finally, it has been reported in literature a role for the lid region in controlling the recognition of p53 by MDM2 and MDMX.[39,40] The lid region is indeed the part of the sequence where the two oncogenic proteins differ the most. This variable region contains several residues of serine and threonine that may be a substrate of the kinases. Taking into

account this observation and on the basis of NMR studies, it has been proposed that the specificity of different kinases for substrates on the lid region may provide a mechanism for MDMX to compete with MDM2 for p53 recognition.[39] Although SCG simulations are not able to give information on the energy associated with the different conformational states of the lid and do not identify any relevant difference in the interactions of this region of MDM2 and MDMX with p53, our study does not exclude such a mechanistic model of competition that, conversely, may complement our results. In view of that, the phosphorylation of the lid region may furnish an additional device to the presence of different conformations and hydrophobic interactions, to finely tune the activity of MDM2 and MDMX.

CONCLUSIONS

The exploration of the conformational transitions featured in the pathway leading from the apo-MDM2 and apo-MDMX states to the p53-bound MDM2 and p53-bound MDMX states has been pursued using spatial coarse graining simulations and adopting the proposed process of protein−protein interaction involving the mechanisms of complex formation and stabilization.[46] The route adopted to move MDM2 and MDMX from the apo-states to the p53-bound states has been defined using the inspection of the experimental structures and the reported experimental data.[33,39,47]

The analysis of the results has enabled us to identify dissimilarities and similarities that regulate the molecular recognition of p53 in the two oncogenic proteins. In particular, the different conformational aspects regulate the binding of p53 in MDM2 and MDMX. These aspects combine with the recently reported smaller binding cleft in the latter protein that forces the assumption of diverse conformations to host the p53 peptide.

MDM2 and MDMX share a similar hydrophobic nature in p53 recognition, with the hydrophobic contacts spanning a wider contact surface than the polar interactions. The pattern, the local shape, and strength of hydrophobic contacts, however, are different in MDM2 and MDMX as evidenced by the FLAP molecular field interaction study. This observation is also sustained by the analysis of the intermolecular interactions, and both data are in agreement with the previously reported experimental results, indicating that the recognition of p53 is favored in MDM2 with respect to MDMX.

Furthermore, a conserved hydrogen bonding interaction is observed between Trp23 of p53 and the backbone of Leu54 in MDM2 and Met53 in MDMX. This hydrogen bond may be envisaged as the directional interaction required for the mechanism of complex formation.

Overall, our results complement the reported role of the lid region of MDM2 and MDMX in controlling the recognition of p53, with its residues of serine and threonine being substrates of different kinases whose diverse specificities provide a mechanism of competition for the two oncogenic proteins.

This study, which provides some novel insights into the mechanism of p53 recognition by MDM2 and MDMX, will be used in approaches for the design of novel dual and selective inhibitors of MDM2 and MDMX that further explore the specific roles of these oncogenic proteins in various cancer types. In addition, the use of different conformations of MDM2 and MDMX for virtual screening purposes may represent an interesting application of this study for the discovery of novel inhibitors of p53/MDM2 and MDMX interaction.

ACKNOWLEDGMENT

This work was supported by the European Union. FP6 PRIORITY LSH-2005-2.2.0-8: Small-ligand libraries: improved tools for exploration and prospective antitumour therapy. DePPICT Project (**De**signing Therapeutic **P** rotein-**P** rotein **I**nhibitors for Brain **C**ancer **T**reatments) Contract number: LSHC-CT-2007- 037834 (http://www.deppict.eu/home.jsp). Dr. Graeme Robertson (Siena Biotech S.p.A.) is gratefully acknowledged for thoughtful suggestions and comments during the preparation of the manuscript.

Supporting Information Available: Clusters of MDM2 and MDMX conformations (Tables s1 and s2), alignment of the p53 binding domains of human MDM2 and human MDMX (Figure s1), results from ANOLEA and Verify3D servers (Figure s2), fluctuations analysis of residues (Figure s3), MDS map of MDM2, MDMX, $MDMX^{Met53Val}$, and $MDMX^{Tyr99Thr}$ (Figure s4), list of atoms belonging to the rigid regions as defined in MDM2, MDMX, and p53 during the simulations, details concerning the use of specific flags in each simulation, and videos of MDM2 and MDMX simulations. This material is available free of charge via the Internet at http://pubs.acs.org.

REFERENCES AND NOTES

(1) Wahl, G. M. Mouse bites dogma: how mouse models are changing our views of how P53 is regulated in vivo. *Cell Death Differ.* **2006**, *13*, 973–983.
(2) Vogelstein, B.; Lane, D.; Levine, A. J. Surfing the p53 network. *Nature* **2000**, *408*, 307–310.
(3) Toledo, F.; Wahl, G. M. Regulating the p53 pathway: in vitro hypotheses, in vivo veritas. *Nat. Rev. Cancer* **2006**, *6*, 909–923.
(4) Chene, P. Inhibiting the p53-MDM2 interaction: an important target for cancer therapy. *Nat. Rev. Cancer* **2003**, *3*, 102–109.
(5) Vousden, K. H.; Lane, D. P. p53 in health and disease. *Nat. Rev. Mol. Cell. Biol.* **2007**, *8*, 275–283.
(6) Lu, F.; Chi, S. W.; Kim, D. H.; Han, K. H.; Kuntz, I. D.; Guy, R. K. Proteomimetic libraries: design, synthesis, and evaluation of p53-MDM2 interaction inhibitors. *J. Comb. Chem.* **2006**, *8*, 315–325.
(7) Lu, Y.; Nikolovska-Coleska, Z.; Fang, X.; Gao, W.; Shangary, S.; Qiu, S.; Qin, D.; Wang, S. Discovery of a nanomolar inhibitor of the human murine double minute 2 (MDM2)-p53 interaction through an integrated, virtual database screening strategy. *J. Med. Chem.* **2006**, *49*, 3759–3762.
(8) Bowman, A. L.; Nikolovska-Coleska, Z.; Zhong, H.; Wang, S.; Carlson, H. A. Small molecule inhibitors of the MDM2-p53 interaction discovered by ensemble-based receptor models. *J. Am. Chem. Soc.* **2007**, *129*, 12809–12814.
(9) Shvarts, A.; Steegenga, W. T.; Riteco, N.; van Laar, T.; Dekker, P.; Bazuine, M.; van Ham, R. C.; van der Houven van Oordt, W.; Hateboer, G.; van der Eb, A. J.; Jochemsen, A. G. MDMX: a novel p53-binding protein with some functional properties of MDM2. *EMBO J.* **1996**, *15*, 5349–5357.
(10) Perry, M. E. Mdm2 in the response to radiation. *Mol. Cancer Res.* **2004**, *2*, 9–19.
(11) Tanimura, S.; Ohtsuka, S.; Mitsui, K.; Shirouzu, K.; Yoshimura, A.; Ohtsubo, M. MDM2 interacts with MDMX through their RING finger domains. *FEBS Lett.* **1999**, *447*, 5–9.
(12) Pan, Y.; Chen, J. MDM2 promotes ubiquitination and degradation of MDMX. *Mol. Cell. Biol.* **2003**, *23*, 5113–5121.
(13) Kawai, H.; Wiederschain, D.; Kitao, H.; Stuart, J.; Tsai, K. K.; Yuan, Z. M. DNA damage-induced MDMX degradation is mediated by MDM2. *J. Biol. Chem.* **2003**, *278*, 45946–45953.
(14) de Graaf, P.; Little, N. A.; Ramos, Y. F.; Meulmeester, E.; Letteboer, S. J.; Jochemsen, A. G. Hdmx protein stability is regulated by the

ubiquitin ligase activity of Mdm2. *J. Biol. Chem.* **2003**, *278*, 38315–38324.
(15) Francoz, S.; Froment, P.; Bogaerts, S.; De Clercq, S.; Maetens, M.; Doumont, G.; Bellefroid, E.; Marine, J. C. Mdm4 and Mdm2 cooperate to inhibit p53 activity in proliferating and quiescent cells in vivo. *Proc. Natl. Acad. Sci. U.S.A.* **2006**, *103*, 3232–3237.
(16) Xiong, S.; Van Pelt, C. S.; Elizondo-Fraire, A. C.; Liu, G.; Lozano, G. Synergistic roles of Mdm2 and Mdm4 for p53 inhibition in central nervous system development. *Proc. Natl. Acad. Sci. U.S.A.* **2006**, *103*, 3226–3231.
(17) Marine, J. C.; Jochemsen, A. G. Mdmx as an essential regulator of p53 activity. *Biochem. Biophys. Res. Commun.* **2005**, *331*, 750–760.
(18) Parant, J.; Chavez-Reyes, A.; Little, N. A.; Yan, W.; Reinke, V.; Jochemsen, A. G.; Lozano, G. Rescue of embryonic lethality in Mdm4-null mice by loss of Trp53 suggests a nonoverlapping pathway with MDM2 to regulate p53. *Nat. Genet.* **2001**, *29*, 92–95.
(19) Migliorini, D.; Lazzerini Denchi, E.; Danovi, D.; Jochemsen, A.; Capillo, M.; Gobbi, A.; Helin, K.; Pelicci, P. G.; Marine, J. C. Mdm4 (Mdmx) regulates p53-induced growth arrest and neuronal cell death during early embryonic mouse development. *Mol. Cell. Biol.* **2002**, *22*, 5527–5538.
(20) Finch, R. A.; Donoviel, D. B.; Potter, D.; Shi, M.; Fan, A.; Freed, D. D.; Wang, C. Y.; Zambrowicz, B. P.; Ramirez-Solis, R.; Sands, A. T.; Zhang, N. mdmx is a negative regulator of p53 activity in vivo. *Cancer Res.* **2002**, *62*, 3221–3225.
(21) Jones, S. N.; Roe, A. E.; Donehower, L. A.; Bradley, A. Rescue of embryonic lethality in Mdm2-deficient mice by absence of p53. *Nature* **1995**, *378*, 206–208.
(22) Montes de Oca Luna, R.; Wagner, D. S.; Lozano, G. Rescue of early embryonic lethality in mdm2-deficient mice by deletion of p53. *Nature* **1995**, *378*, 203–206.
(23) Marine, J. C.; Francoz, S.; Maetens, M.; Wahl, G.; Toledo, F.; Lozano, G. Keeping p53 in check: essential and synergistic functions of Mdm2 and Mdm4. *Cell Death Differ.* **2006**, *13*, 927–934.
(24) Toledo, F.; Krummel, K. A.; Lee, C. J.; Liu, C. W.; Rodewald, L. W.; Tang, M.; Wahl, G. M. A mouse p53 mutant lacking the proline-rich domain rescues Mdm4 deficiency and provides insight into the Mdm2-Mdm4-p53 regulatory network. *Cancer Cell.* **2006**, *9*, 273–285.
(25) Ramos, Y. F.; Stad, R.; Attema, J.; Peltenburg, L. T.; van der Eb, A. J.; Jochemsen, A. G. Aberrant expression of HDMX proteins in tumor cells correlates with wild-type p53. *Cancer Res.* **2001**, *61*, 1839–1842.
(26) Laurie, N. A.; Donovan, S. L.; Shih, C. S.; Zhang, J.; Mills, N.; Fuller, C.; Teunisse, A.; Lam, S.; Ramos, Y.; Mohan, A.; Johnson, D.; Wilson, M.; Rodriguez-Galindo, C.; Quarto, M.; Francoz, S.; Mendrysa, S. M.; Guy, R. K.; Marine, J. C.; Jochemsen, A. G.; Dyer, M. A. Inactivation of the p53 pathway in retinoblastoma. *Nature* **2006**, *444*, 61–66.
(27) Hu, B.; Gilkes, D. M.; Chen, J. Efficient p53 activation and apoptosis by simultaneous disruption of binding to MDM2 and MDMX. *Cancer Res.* **2007**, *67*, 8810–8817.
(28) Hu, B.; Gilkes, D. M.; Farooqi, B.; Sebti, S. M.; Chen, J. MDMX overexpression prevents P53 activation by the MDM2 inhibitor nutlin. *J. Biol. Chem.* **2006**, *281*, 33030–33035.
(29) Patton, J. T.; Mayo, L. D.; Singhi, A. D.; Gudkov, A. V.; Stark, G. R.; Jackson, M. W. Levels of HdmX expression dictate the sensitivity of normal and transformed cells to Nutlin-3. *Cancer Res.* **2006**, *66*, 3169–3176.
(30) Wade, M.; Wong, E. T.; Tang, M.; Vassilev, L. T.; Wahl, G. M. Hdmx modulates the outcome of p53 activation in human tumor cells. *J. Biol. Chem.* **2006**, *281*, 33036–33044.
(31) Popowicz, G. M.; Czarna, A.; Rothweiler, U.; Sszwagierczak, A.; Krajewski, M.; Weber, L.; Holak, T. A. Molecular Basis for the Inhibition of p53 by Mdmx. *Cell Cycle* **2007**, *6*, 2386–2392.
(32) Schrodinger, L. C. C. *Maestro*; New York, NY, 2005.
(33) Uhrinova, S.; Uhrin, D.; Powers, H.; Watt, K.; Zheleva, D.; Fischer, P.; McInnes, C.; Barlow, P. N. Structure of free MDM2 N-terminal domain reveals conformational adjustments that accompany p53-binding. *J. Mol. Biol.* **2005**, *350*, 587–598.
(34) Grasberger, B. L.; Lu, T.; Schubert, C.; Parks, D. J.; Carver, T. E.; Koblish, H. K.; Cummings, M. D.; LaFrance, L. V.; Milkiewicz, K. L.; Calvo, R. R.; Maguire, D.; Lattanze, J.; Franks, C. F.; Zhao, S.; Ramachandren, K.; Bylebyl, G. R.; Zhang, M.; Manthey, C. L.; Petrella, E. C.; Pantoliano, M. W.; Deckman, I. C.; Spurlino, J. C.; Maroney, A. C.; Tomczuk, B. E.; Molloy, C. J.; Bone, R. F. Discovery and cocrystal structure of benzodiazepinedione HDM2 antagonists that activate p53 in cells. *J. Med. Chem.* **2005**, *48*, 909–912.
(35) Xiang, Z.; Honig, B. Extending the accuracy limits of prediction for side-chain conformations. *J. Mol. Biol.* **2001**, *311*, 421–430.
(36) Davis, I. W.; Leaver-Fay, A.; Chen, V. B.; Block, J. N.; Kapral, G. J.; Wang, X.; Murray, L. W.; Arendall, W. B., III; Snoeyink, J.; Richardson, J. S.; Richardson, D. C. MolProbity: all-atom contacts and structure validation for proteins and nucleic acids. *Nucleic Acids Res.* **2007**, *35*, W375−383.
(37) Melo, F.; Feytmans, E. Assessing protein structures with a non-local atomic interaction energy. *J. Mol. Biol.* **1998**, *277*, 1141–1152.
(38) Luthy, R.; Bowie, J. U.; Eisenberg, D. Assessment of protein models with three-dimensional profiles. *Nature* **1992**, *356*, 83–85.
(39) McCoy, M. A.; Gesell, J. J.; Senior, M. M.; Wyss, D. F. Flexible lid to the p53-binding domain of human Mdm2: implications for p53 regulation. *Proc. Natl. Acad. Sci. U.S.A.* **2003**, *100*, 1645–1648.
(40) Showalter, S. A.; Bruschweiler-Li, L.; Johnson, E.; Zhang, F.; Bruschweiler, R. Quantitative lid dynamics of MDM2 reveals differential ligand binding modes of the p53-binding cleft. *J. Am. Chem. Soc.* **2008**, *130*, 6472–6478.
(41) Gohlke, H.; Thorpe, M. F. A natural coarse graining for simulating large biomolecular motion. *Biophys. J.* **2006**, *91*, 2115–2120.
(42) Van Der Spoel, D.; Lindahl, E.; Hess, B.; Groenhof, G.; Mark, A. E.; Berendsen, H. J. GROMACS: fast, flexible, and free. *J. Comput. Chem.* **2005**, *26*, 1701–1718.
(43) De Leeuw, J. Applications of Convex Analysis to Multidimensional Scaling. In *Recent Developments in Statistics*; Barra, J. R. a. o., Ed.; North Holland Publishing Company: Amsterdam, The Netherlands, 1977; pp 133−146.
(44) Wallace, A. C.; Laskowski, R. A.; Thornton, J. M. LIGPLOT: a program to generate schematic diagrams of protein-ligand interactions. *Protein Eng.* **1995**, *8*, 127–134.
(45) Baroni, M.; Cruciani, G.; Sciabola, S.; Perruccio, F.; Mason, J. S. A common reference framework for analyzing/comparing proteins and ligands. Fingerprints for Ligands and Proteins (FLAP): theory and application. *J. Chem. Inf. Model.* **2007**, *47*, 279–294.
(46) Archakov, A. I.; Govorun, V. M.; Dubanov, A. V.; Ivanov, Y. D.; Veselovsky, A. V.; Lewi, P.; Janssen, P. Protein-protein interactions as a target for drugs in proteomics. *Proteomics* **2003**, *3*, 380–391.
(47) Kussie, P. H.; Gorina, S.; Marechal, V.; Elenbaas, B.; Moreau, J.; Levine, A. J.; Pavletich, N. P. Structure of the MDM2 oncoprotein bound to the p53 tumor suppressor transactivation domain. *Science* **1996**, *274*, 948–953.

CI800146M